ФИЗИКА ЭЛЕМЕНТАРНЫХ ЧАСТИЦ И АТОМНОГО ЯДРА. ТЕОРИЯ

THERMAL DESCRIPTION OF PARTICLE PRODUCTION IN Au–Au COLLISIONS AT STAR ENERGIES

A. Tawfik[1], *E. Abbas*[2]

Egyptian Center for Theoretical Physics (ECTP), Modern University for Technology
and Information (MTI), Cairo

World Laboratory for Cosmology and Particle Physics (WLCAPP), Cairo

The hadron ratios measured in central Au–Au collisions are analyzed by means of the Hadron Resonance Gas (HRG) model over a wide range of nucleon–nucleon center-of-mass energies, $\sqrt{s_{NN}} = 7.7 - 200$ GeV as offered by the STAR Beam Energy Scan I (BES-I). The temperature and baryon chemical potential are deduced from fits of experimental ratios to thermal model calculations assuming chemical equilibrium. We find that the resulting freeze-out parameters using single hard-core value and point-like constituents of HRG are identical. This implies that the excluded volume comes up with no effect on the extracted parameters. We compare the results with other studies and with the lattice QCD calculations. Various freeze-out conditions are confronted with the resulting data set. The effect of including new resonances is also analyzed. At vanishing chemical potential, a limiting temperature was estimated, $T_{\lim} = (158.5 \pm 3)$ MeV.

В работе проанализированы отношения выходов адронов в центральных столкновениях Au–Au в рамках модели адронного резонансного газа (АРГ) в широкой области энергий центра масс системы нуклон–нуклон — $\sqrt{s_{NN}} = 7{,}7 - 200$ ГэВ, как было предложено в процессе сканирования по энергиям пучка I коллаборацией STAR (BES-I). Температура и барионный химический потенциал получены из фитирования экспериментальных отношений из вычислений в рамках тепловых моделей в предположении химического равновесия. Показано, что параметры вымораживания, получаемые с помощью только величины жесткого кора и точечных конституэнтов АРГ, идентичны. Это означает, что неучет размеров конституэнтов не влияет на величину извлекаемых параметров. Полученные результаты сравниваются с другими моделями и вычислениями КХД на решетке. Рассмотрены различные условия вымораживания, и исследовано их влияние на получаемые результаты. Также рассмотрен эффект учета новых резонансов. Показано, что при исчезающе малом химическом потенциале достигается предельная температура $T_{\lim} = (158{,}5 \pm 3)$ МэВ.

PACS: 24.10.Pa; 25.75.Dw; 12.38.Mh

INTRODUCTION

The heavy-ion experiments are carried out to study hadronic matter under extreme conditions of high temperature and/or density [1]. These conditions likely exist in the core of compact neutron stars and should be established a few microseconds after the Big Bang,

---

[1] http://www.atawfik.net/; e-mail: a.tawfik@eng.mti.edu.eg

[2] E-mail: e.gamal@eng.mti.edu.eg

when matter was in its primordial state, a soup of Quark-Gluon Plasma (QGP). Data from the Relativistic Heavy-Ion Collider (RHIC) have shown that QGP, the new state of matter, was created in Au–Au collisions [2]. It is conjectured that the created hot and dense partonic matter rapidly expands and cools down. On path of this evolution, it undergoes phase transition(s) back to the hadronic matter. Different thermal models [3–10] can very well reproduce the particle abundances, which are governed in final state — at chemical equilibrium — by two parameters, the chemical freeze-out temperature T_{ch} and the baryon chemical potential μ_b, where the latter reflects the net baryon content of the system. Different values of T_{ch} and μ_b at different energies set up the chemical freeze-out line. This line appears very close to the phase boundary between QGP and hadronic phase, especially at low μ_b.

To explore the freeze-out diagram preciously, gap in the energies between old RHIC and top Superproton Synchrotron (SPS) should be filled. Therefore, the Solenoidal Tracker At RHIC (STAR) launched first phase of the Beam Energy Scan (BES-I) program [11], in order to collect data from $Au+Au$ collisions at center-of-mass energies of 39, 27, 19.6, 11.5, and 7.7 GeV covering a wide range of baryon chemical potential ~ 100–400 MeV in the Quantum Chromodynamics (QCD) phase diagram [11]. Within this energy range, two important features are conjectured to be populated, the critical endpoint and closeness between LQCD phase transition and chemical freeze-out.

In the present work, the freeze-out parameters, T_{ch} and μ_b, are extracted from fits of the experimental particle ratios with corresponding ratios calculated in the HRG model assuming chemical equilibrium. The experimental hadron ratios are limited to mid-rapidity central Au–Au collisions at energies 200, 130, 62.4, 39, 11.5, 7.7 GeV. The contributions of weak decay feed-down and effects of cut-off on hadron resonances have been studied. The results are compared with recent lattice QCD pseudocritical temperature $T_{\mathrm{ch}} = (154 \pm 9)$ MeV, which has been estimated at vanishing chemical potential [12].

The present paper is organized as follows. Section 1 elaborates details about the HRG model. The hadron interactions, excluded-volume correction are discussed also in Subsec. 1.2. The fits of the experimental ratios with the HRG calculations are discussed in Sec. 2. Section 3 is devoted to the results and discussion. The conclusions and outlook are summarized in the last section.

1. THE MODEL

1.1. Hadron Resonance Gas. According to Hagedorn [13], the hadronic phase is assumed to have large degrees of freedom. Additionally, there should be a kind of equilibrium. Therefore, statistical mechanics can be used in describing this phase. In nuclear collisions, the formation of hadrons at chemical freeze-out temperature T_{ch} should be controlled by the phase space and conservation laws. The phase space of each particle depends on the energy, degeneracy and available volume. For a large number of produced particles, Grand Canonical Ensemble (GCE) is justified. The grand canonical partition function reads

$$Z(T, \mu, V) = \mathrm{Tr} \left[\exp \left(\frac{\mu N - H}{T} \right) \right], \tag{1}$$

where H is the Hamiltonian of the system and T (μ) being the temperature (chemical potential). The Hamiltonian is given by the sum of the kinetic energies of the relativistic Fermi

and Bose particles. The main motivation of using this Hamiltonian is that it contains all relevant degrees of freedom of confined and strongly interacting matter. It includes implicitly the interactions that result in resonance formation [14–19]. With the above assumptions the dynamics of the partition function can be calculated exactly and can be expressed as a sum over *single-particle partition* functions Z_i^1 of stable hadrons and their resonances

$$\ln Z(T, \mu, V) = \sum_i \ln Z_i^1(T, V) = \sum_i \pm \frac{V g_i}{2\pi^2} \int_0^\infty p^2 dp \ln \left\{ 1 \pm \exp \left[\frac{\mu_i - \varepsilon_i(p)}{T} \right] \right\}, \quad (2)$$

where $\varepsilon_i(p) = (p^2 + m_i^2)^{1/2}$ is the ith particle dispersion relation, g_i is the spin–isospin degeneracy factor and $\pm$ stands for fermions and bosons, respectively. The ith particle chemical potential is given as $\mu_i = \mu_b B_i + \mu_s S_i + \mu_{I^3} I_i^3$, where B_i, S_i and I_i^3 are the baryon, strange and isospin quantum number, respectively. The thermodynamic properties of the system can be obtained from the partition function of all resonances in the hadronic phase.

At finite temperature T and baryon chemical potential μ_i, the pressure of the ith hadron or resonance species reads

$$p(T, \mu_i) = \pm \frac{g_i}{2\pi^2} T \int_0^\infty p^2 dp \ln \left\{ 1 \pm \exp \left[\frac{\mu_i - \varepsilon_i(p)}{T} \right] \right\}. \quad (3)$$

As no phase transition is conjectured in HRG, summing over all hadron resonances results in the final thermodynamic pressure. The number density can be obtained as

$$n(T, \mu) = \sum_i \frac{\partial}{\partial \mu_i} p(T, \mu_i) = \sum_i \frac{g_i}{2\pi^2} \int_0^\infty \frac{p^2 dp}{\exp \left[\frac{\mu_i - \varepsilon_i(p)}{T} \right] \pm 1}. \quad (4)$$

The conservation laws should be fulfilled throughout the chemical potentials and temperature. They include conservation of strangeness $V \sum_i n_i(T, \mu_i) S_i = 0$ (vanishing strangeness), baryon, $V \sum_i n_i(T, \mu_i) B_i = Z + N$ (conserved charge and baryon number) and isospin, $V \sum_i n_i(T, \mu_i) I_i^3 = (N - Z)/2$, where N and Z are the neutron and proton number in the colliding nuclei.

For completeness, it is worthwhile to mention that the degree of nonequilibrium can be implemented — among others — through the strange quark occupation factor γ_s (and may be also that of light quarks γ_q) [20, 21] in the partition function

$$\ln Z(T, \mu, V, \gamma_s) = \sum_i \pm \frac{V g_i}{2\pi^2} \int_0^\infty p^2 dp \ln \left(1 \pm \gamma_s^{s_i} \exp \left[\frac{\mu_i - \varepsilon_i(p)}{T} \right] \right), \quad (5)$$

where s_i is the number of strange valence quarks and antiquarks in the ith hadron. The value of γ_s is always less than unity in proton–proton (pp) [22,23] and electron–positron ($e^- e^+$) [24] interactions. This apparently points to strangeness phase space suppression in elementary collisions.

During the final expansion, the main process at this stage is unstable resonance decay. So, the final number density for the ith particle is given as

$$n_i^{\text{fin}} = n_i + \sum_j \text{Br}_{j \to i} n_j, \tag{6}$$

where $\text{Br}_{j \to i}$ is the effective branching ratio of the jth hadron resonance into the ith particle. Taking into consideration all multistep decay cascades, we have

$$\text{Br}_{j \to i} = \text{br}_{j \to i} + \sum_{l_1} \text{br}_{j \to l_1} \text{br}_{l_1 \to i} + \sum_{l_1, l_2} \text{br}_{j \to l_1} \text{br}_{l_1 \to l_2} \text{br}_{l_2 \to i} + \ldots, \tag{7}$$

where $\text{br}_{j \to i}$ is the branching ratio of the jth hadron resonance into the ith hadron.

In the present work, we include contributions of the hadrons, which consist of light flavors particles listed by the Particle Data Group (PDG) [26]. The decay branching ratios are also taken from [26]. For the observed decay channels with unknown probabilities, we follow the rules given in [27]. The zero-width approximation is utilized, because including the widths leads to large numerical costs and the less improvement in the final results [4, 28, 29], particularly at energies higher than that of the Alternating Gradient Synchrotron (AGS) energies. The excluded-volume correction (EVC) [10] is applied taking into account the volume occupied by individual hadrons with radii r_m for mesons and r_b for baryons. The thermodynamic quantities are modified due to EVC. The corrected pressure will be obtained by an iterative procedure

$$p^{\text{excl}}(T, \mu_i) = p^{\text{id}}(T, \tilde{\mu}_i), \quad \tilde{\mu}_i = \mu_i - \upsilon p^{\text{excl}}(T, \tilde{\mu}_i), \tag{8}$$

where $p^{\text{id}}(p^{\text{excl}})$ being the pressure in the ideal case (case of excluded volume) and υ is the *eigen* volume, which is calculated for any hard-core radius r by $16\pi r^3/3$ [30]. The framework of GCE assuming full chemical equilibrium, i.e., $\gamma_s = 1$, is the one, which we utilize in the present analysis.

1.2. Hadron Interactions and Excluded-Volume Correction. In the present work, we concentrate on the van der Waals repulsive interaction between hadrons, which can be implemented as hard core [10]. Assuming that hadrons have spherical hard core, a considerable modification in the thermodynamic quantities of the ideal hadron gas takes place. Based on nucleon–nucleon scattering, the nucleon should have a hard core of radius of approximately 0.3 fm. The main question is what about the other resonances hard core? In literature [9, 32], we find a wide spectrum of hard-core radii ranging from 0.0 and 0.8 fm. As an attempt to solve this problem, Tawfik [31] confronted various thermodynamic quantities calculated in HRG with different hadron radii to the first principle lattice QCD simulations [33]. Using one hard-core radius for all hadrons, it has been concluded that increasing the hard-core radius reduces the ability to reproduce the lattice QCD calculations. At $0 \leqslant r < 0.2$ fm, the ability of the HRG model to reproduce the lattice energy density or trace anomaly at low temperature (hadronic phase) is very high. Thus, we restrict the hard-core radius to small values.

In the present work, we estimate the freeze-out parameters in HRG with the point-like and same finite hard-core radius, $r = 0.3$ fm, for both mesons and baryons.

2. FIT WITH PARTICLE RATIOS

From N experimental hadron yields, $N - 1$ statistically-independent ratios can be constructed. Assuming full chemical equilibrium in thermal models, just two parameters should be estimated in order to reproduce the experimental data. The present work is devoted to these thermal parameters, T_{ch} and μ_b. Therefore, fitting the HRG results with the experimental ratios determines the statistically-best parameters. Other methods, such as the fitting to the measured hadron yields [34], can be used to deduce another parameter, the fireball volume. Unstable resonance states like ϕ and K^* will be avoided because of rescattering and regeneration [35], which likely happened during the later expansion after the chemical freeze-out.

At RHIC energies, the rapidity distribution exhibits a boost-invariant plateau near mid-rapidity [36]. As demonstrated in [37], the effects of hydrodynamic flow would be cancelled out in the particle ratios. Therefore, the measurements at mid-rapidity are consistent with the framework of the HRG model, which does not contain any dynamical treatment. For our analysis, the most-central collisions are strongly recommended, especially when the statistical treatment is based on GCE. The contributions of weak decays were implemented in the HRG model in order to match with the experimental conditions. The analysis includes 11 (occasionally 10) independent particle ratios. The set of particle ratios is kept unchanged at all energies as possible.

The criterion for the best statistical fitting is based on estimating minima, for instance,

$$\chi^2 = \sum_i \frac{\left(R_i^{\text{exp}} - R_i^{\text{model}}\right)^2}{\sigma_i^2}, \tag{9}$$

and quadratic deviation

$$q^2 = \sum_i \frac{\left(R_i^{\text{exp}} - R_i^{\text{model}}\right)^2}{\left(R_i^{\text{model}}\right)^2}, \tag{10}$$

where R_i^{exp} (R_i^{model}) is the ith measured (calculated) ratio and σ is the experimental data error. Both methods, χ^2 and q^2, are implemented. Any possible deviation between these two methods should give an indication about the accuracy of the parameters extracted from the given data set. The statistically-independent ratios used in estimating χ^2 and q^2 at 200, 130 and 62.4 GeV are π^-/π^+, K^-/K^+, $\bar{p}/p$, $\bar{\Lambda}/\Lambda$, $\bar{\Xi}/\Xi$, $\bar{\Omega}/\Omega$, K^-/π^-, $\bar{p}/\pi^-$, Λ/π^-, Ξ/π^- and Ω/π^-. Except for 200 GeV, we also use $(\Omega + \bar{\Omega})/\pi^-$ instead of Ω/π^-, i.e., 11 particle ratios. At 39, 11.5 and 7.7 GeV, π^-/π^+, K^-/K^+, $\bar{p}/p$, $\bar{\Lambda}/\Lambda$, $\bar{\Xi}/\Xi$, $\bar{\Omega}/\Omega$, K^-/π^-, $\bar{p}/\pi^-$, Λ/π^- and $\bar{\Xi}/\pi^-$, i.e., 10 particle ratios are used. Additional ratios may be used, but only in figures. Further details about the given data sets at various STAR energies are in order.

At 200 GeV, we use yields of pions, kaons, (anti)protons [38], (anti)lambda and multistrange baryons [39, 40] measured at mid-rapidity in STAR experiment at centrality 0–5%, except the $\Omega/\bar{\Omega}$ ratios, which were measured at 0–20% [40]. The measured pions spectra are corrected for feed-down from weak decays, as well as Λ ($\bar{\Lambda}$) are corrected for feed-down from weak decays of multistrange baryons. The comparison between the experimental (symbols) and calculated (horizontal lines) ratios is shown in Fig. 1, *a*.

At 130 GeV, we use yields of pions, kaons, (anti)protons [38], (anti)lambda [41] and multistrange baryons [40, 42] measured at mid-rapidity in STAR experiment at centrality
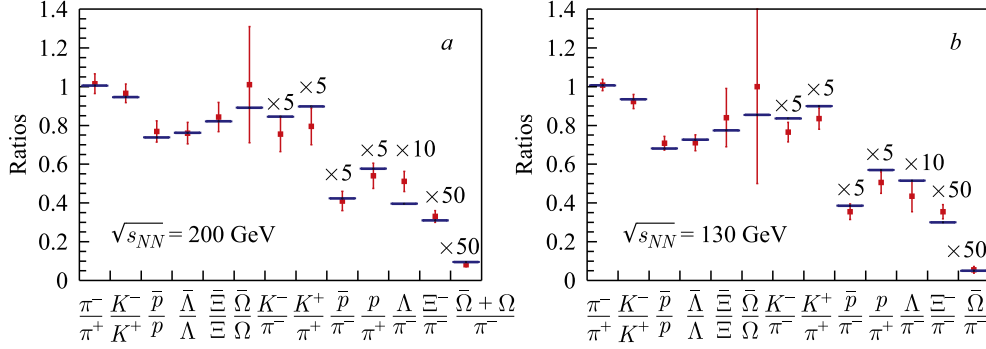
Fig. 1. *a*) The experimental particle ratios (symbols) [38–40] are compared to the HRG calculations (horizontal lines) at 200 GeV, where the latter were performed at $T_{\rm ch}$ and μ_b parameters, which assure minimum χ^2. For comparison with other ratios and better appearance, some ratios are scaled (scaling factor is given), so that we avoid log plotting. *b*) The same as in plot *a*, but at 130 GeV, where the experimental particle ratios are taken from [38, 40–42]

0–5%, except the multistrange baryons, which have been measured at 0–20%. The measured pions spectra are corrected for feed-down from weak decays. The results comparing the STAR with HRG ratios are shown in Fig. 1, *b*.

At 62.4 GeV, we use yields of pions, kaons, (anti)protons [38], (anti)lambda and multi-strange baryons [40] measured at mid-rapidity in STAR experiment at centrality 0–5%, except the multistrange baryons, which were measured at 0–20%. The measured pions spectra are corrected for feed-down from weak decays, as well as Λ ($\bar{\Lambda}$) are corrected for feed-down from weak decays of Ξ. The comparison between the STAR and HRG results is shown in Fig. 2, *a*.

At 39, 11.5 and 7.7 GeV, we use yields of pions, kaons, (anti)protons [43, 44], Λ, $\bar{\Lambda}$, Ξ and $\bar{\Xi}$ [45] measured at mid-rapidity in STAR experiment at centrality 0–5%. The $\Omega/\bar{\Omega}$ ratios have been measured at centrality 0–5, 0–20 and 0–60% for 39, 11.5 and 7.7 GeV, respectively [46]. The measured pions spectra have been corrected for feed-down from weak decays, as well as Λ ($\bar{\Lambda}$) — for the feed-down contributions from Ξ weak decay. The
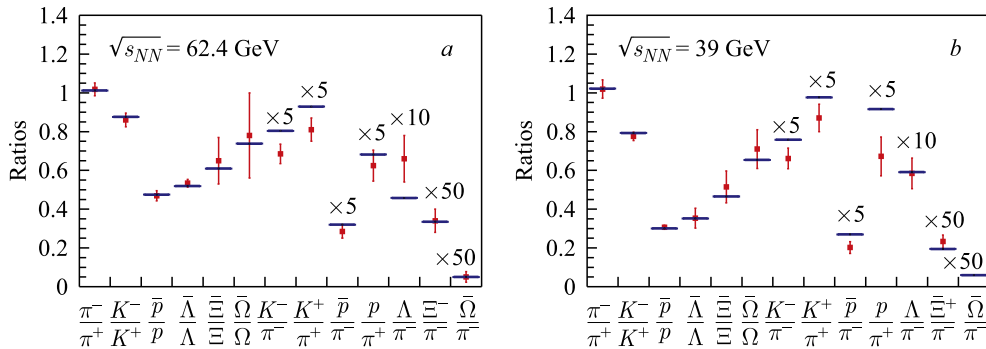

Fig. 2. The same as in Fig. 1, *a*, but at 62.4 GeV (*a*), where the experimental particle ratios are taken from [38, 40], and at 39 GeV (*b*), where the experimental particle ratios are taken from [43–46]
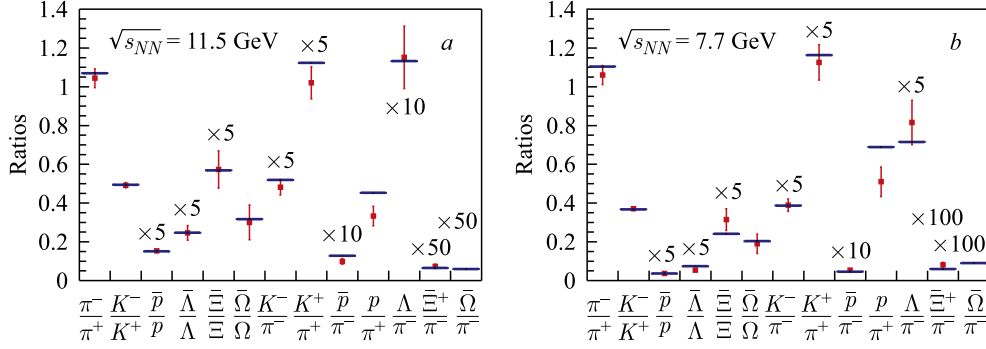
Fig. 3. The same as in Fig. 1, *a*, but at 11.5 (*a*) and 7.7 GeV (*b*), where experimental data are taken from [43–46]

analysis includes 10 independent ratios, where Ω/π was not included. The results are shown in Fig. 2, *b* and Fig. 3.

The freeze-out parameters, $T_{\rm ch}$ and μ_b, are estimated from χ^2 and q^2 fitting approaches assuming point-like and finite hard-core radius ($r_m = r_b = 0.3$ fm). The results are listed out in Table 1. A few remarks are now in order.

• The difference between the freeze-out parameters extracted from the HRG model with vanishing and finite hard core is too small.

• The same behaviour of the extracted parameters is also observed in both χ^2 and q^2 on $\sqrt{s_{NN}}$, although the parameters extracted using q^2 are a little bit larger than the ones using χ^2/dof. This reflects the accuracy of extracted parameters.

• The main difference between both fitting methods is that χ^2 takes into consideration the uncertainty of the experiment. In χ^2/dof, not only the ratios, which are sensitive to $T_{\rm ch}$ and μ_b, will have the upper hand in determining the extracted parameters, but also the ratios with higher measured accuracy. On the other hand, q^2 is designed to reflect the deviation. Therefore, χ^2/dof seems to be more suitable to be implemented.

• It is obvious that the values of χ^2/dof are close to unity, except at 7.7 GeV. The reason may be the need to assume a degree of nonequilibrium, especially at this relative low energy.

Table 1. **At STAR energies, the freeze-out parameters, $T_{\rm ch}$ and μ_b, are estimated from χ^2 and q^2 fitting approaches assuming point-like and finite hard-core raduis ($r_m = r_b = 0.3$ fm). In both fittings, the degrees of freedom (dof) are given**

$\sqrt{s_{NN}}$, GeV	$r_m = r_b = 0.0$ fm						$r_m = r_b = 0.3$ fm					
	$T_{\rm ch}$	μ_b	χ^2/dof	$T_{\rm ch}$	μ_b	q^2	$T_{\rm ch}$	μ_b	χ^2/dof	$T_{\rm ch}$	μ_b	q^2
200	159.5	27.5	9.24/9	161.5	30	0.137	159.5	27.5	9.24/9	161.5	29.5	0.137
130	157.5	34	6.86/9	160	32	0.108	157	34	7.07/9	159.5	32	0.109
62.4	157.5	66.5	10.17/9	161.5	73	0.185	157	66	10.51/9	161.5	72.5	0.185
39	160.5	110.5	10.69/8	163.5	113.5	0.122	160.5	110.5	11.03/8	163	112.5	0.124
11.5	153	308	6.06/8	153.5	312	0.072	153	308	6.28/8	153	310	0.073
7.7	145.5	410.5	15.21/8	149	412.5	0.265	145	409	15.07/8	148.5	419	0.263

Table 2. **The freeze-out parameters estimated from χ^2/dof best fit of various experimental particle ratios in the HRG framework with $r_m = r_b = 0.0$ fm**

$\sqrt{s_{NN}}$, GeV	T_{ch}, MeV	μ_b, MeV
200	159.5 ± 2	27.5 ± 4
130	157.5 ± 4	34 ± 3.5
62.4	157.5 ± 3.5	66.5 ± 4
39	160.5 ± 3.5	110.5 ± 4.5
11.5	153 ± 1.5	308 ± 2.5
7.7	145.5 ± 1	410.5 ± 4

Depending on the previous notes, we focus on the results of χ^2/dof method taking $\sim 1\sigma$-error at $r_m = r_b = 0.0$ fm. The final results are summarized in Table 2.

3. RESULTS AND DISCUSSION

3.1. Effects of Excluded-Volume Correction (EVC). The differences between extracted thermal parameters using finite hard core for hadrons ($r_m = r_b = 0.3$ fm) and the vanishing one ($r_m = r_b = 0.0$ fm) are nearly negligible. Actually, if one uses Maxwell–Boltzmann statistics, the number density of the ith particle will be suppressed by R_i, Eq. (12), [10]:

$$n_i^{\mathrm{excl}}(T, \mu_i) = R_i n_i^{\mathrm{id}}(T, \mu_i), \tag{11}$$

where

$$R_i(T, \mu_i, v) = \frac{\exp\left(\dfrac{-v_i p^{\mathrm{excl}}}{T}\right)}{1 + \sum_i v_i n_i^{\mathrm{id}}(T, \tilde{\mu}_i)}. \tag{12}$$

Then, the ratios between two particle species at finite excluded volume will be

$$\frac{n_i^{\mathrm{excl}}(T, \mu_i)}{n_j^{\mathrm{excl}}(T, \mu_i)} = \frac{R_i n_i^{\mathrm{id}}(T, \mu_i)}{R_j n_j^{\mathrm{id}}(T, \mu_i)}. \tag{13}$$

Therefore, the ratios should not be effected, when $r_m = r_b$. In the present paper, we use quantum statistics, which makes a very small shift in the extracted thermal parameters. Both sides of Eq. (13) are not exactly equal, but still represent a good approximation.

As given in Table 1, although the effect of EVC on the extracted thermal parameters can be completely ignored, when $r_m = r_b$, the effect would increase when different hard-core radii for mesons and baryons ($r_m \neq r_b$) are assumed. The effect of EVC appears in thermodynamic quantities, like energy, entropy and number densities, as seen in Eq. (11).

3.2. Effects of Weak Decay from Feed-Down. The contribution of feed-down from weak decay has been studied in [4]. Accordingly, the energy dependence of the contribution of weak decays to yields of pions, protons and hyperons was parameterizations in terms of the freeze-out parameters, T_{ch} and μ_b. Concretely, the fraction of the total yield of these particles is conjectured to stem from weak decays. It has been noticed that this quantity reaches some asymptotic values, 15, 25 and 35% for pion, lambda and proton, respectively. For antiparticles

at high energies, such values should be significantly large [4]. It has been found that assuming different contributions from feed-down from weak decay leads to different extracted thermal parameters [4, 27].

3.3. Effects of Including New Resonances. The discovery of new hadron resonances apparently affects the values of extracted freeze-out parameters, T_{ch} and μ_b [47].

• We have repeated the analysis without σ labelled as $f_0(600)$ aiming to estimate its effect on the freeze-out parameters at 200 and 130 GeV. We get $\mu_b = 27$, and $T_{\mathrm{ch}} = 157$ MeV at 200 GeV and $\mu_b = 33.5$, $T_{\mathrm{ch}} = 154.5$ MeV at 130 GeV. Comparing these with the corresponding ones in Table 2 ($\mu_b = 27.5$, $T_{\mathrm{ch}} = 159.5$ MeV and $\mu_b = 34$, $T_{\mathrm{ch}} = 157.5$ MeV, respectively) shows that the effect of including σ is relatively effective.

• We have repeated the analysis at 200 and 130 GeV, when resonance masses $\leqslant 2$ GeV. The same results were obtained.

We conclude that the discovery of new particles (especially the light ones like σ) would affect the extracted freeze-out parameters.

3.4. Energy Dependence of the Freeze-Out Parameters. Estimating different freeze-out parameters at different energies raises the question about the systematic energy dependence. In Fig. 4, we compare our results with the previous studies [4, 47]. The dependence of the extracted μ_b on $\sqrt{s_{NN}}$, Fig. 4, *a*, can be parameterized as

$$\mu_b(\mathrm{GeV}) = \frac{a}{1 + b\sqrt{s_{NN}}(\mathrm{GeV})}, \tag{14}$$

where $a = (1.245 \pm 0.094)$ GeV and $b = (0.264 \pm 0.028)$ GeV^{-1}, which are represented as a dashed curve in Fig. 4, *a*. The corresponding values coincide with those obtained in [4] within the error bands.
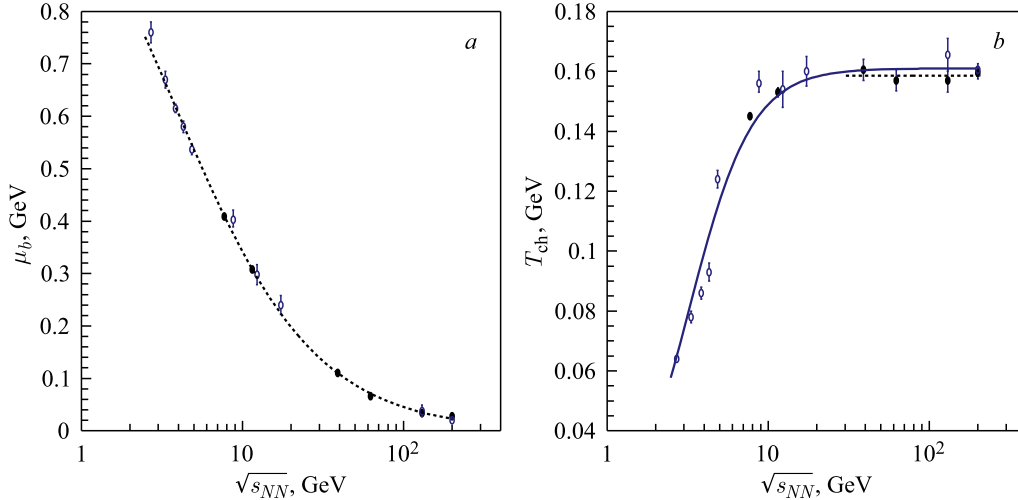

Fig. 4. The energy dependence of the extracted parameters μ_b (*a*) and T_{ch} (*b*). The open symbols represent results of [4], which are extracted by the same criteria (minimizing χ^2/dof). The closed symbols give the results of this paper. The dashed curve (*a*) stands for Eq. (14). The dashed line (*b*) gives the best fit of four relative high-energy points (see the text), whereas the solid line (*b*) represents Eq. (15)

Also, the dependence of T_{ch} on $\sqrt{s_{NN}}$ can be parameterized [47]:

$$T_{\text{ch}} = T_{\text{lim}} \left(\frac{1}{1 + \exp\left[\dfrac{1.172 - \ln\left(\sqrt{s_{NN}}\right)}{0.45}\right]} \right), \tag{15}$$

where $\sqrt{s_{NN}}$ are given in GeV. The limiting temperature reads, $T_{\text{lim}} = 161$ MeV. We have so-far estimated just six points. The range of the extracted temperatures is relatively small, which would not be enough to construct parameterization as given in Eq. (15). However, the new results can give a better estimation for T_{lim}, where the temperature is approximately constant at relative high energy (200, 130, 62.4 and 39 GeV). Taking the average of these four points, we have $T_{\text{lim}} = (158.5 \pm 3)$ MeV (dashed line in Fig. 4, *b*).

3.5. Comparing Results with Other Works and LQCD. Figure 5 shows the dependence of T_{ch} on μ_b, the freeze-out diagram. The results of [4, 25, 38] are compared with that of the present analysis. Also, the results taken from [25] were obtained using statistical hadronization model with partial chemical equilibrium ($\gamma_s \neq 1$). The STAR points [38] were obtained using the particle ratios, in which strange baryons ratios were not included. The comparison shows a consistency between the extracted parameters of BES-I (the present work) with the old RHIC and SPS [4, 25, 38].
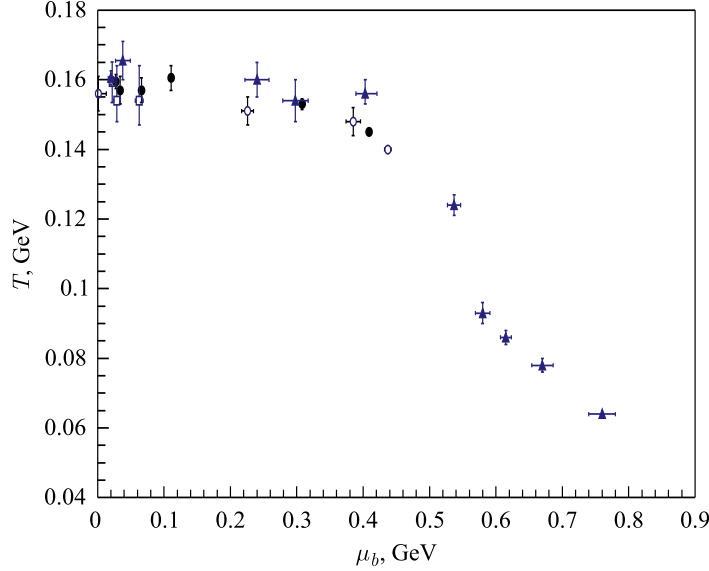

Fig. 5. The regularities in the extracted thermal parameters are shown in the freeze-out diagram. The closed diamond symbols are the results from [4], the open circle symbols are the results from [25], the open square is the STAR results (at 0–5% centrality) [38] and the closed symbols are the new result of our analysis. Within the range covered by the present analysis, the agreement is convincing
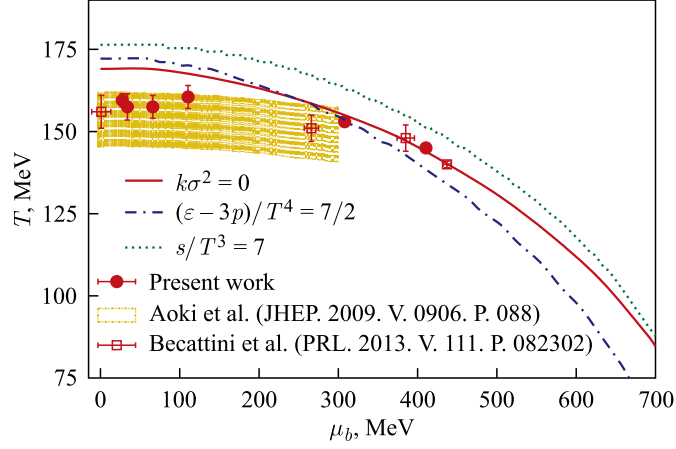
Fig. 6. The freeze-out parameters are compared with the lattice QCD calculations (band) [12, 48]

In Fig. 6, lattice QCD pseudocritical temperature [12] and its leading-order correction in μ_b/T [48] are confronted with the HRG model parameters in Table 2 showing closeness of chemical freeze-out and the QCD transition line at relatively low μ_b.

CONCLUSIONS

Over the last three decades, heavy-ion experiments at energies ranging from SIS and LHC have been carried out. Different measurements of particle ratios at ALICE, RHIC, SPS, AGS and SIS revealed the thermal parameters (T_{ch} and μ_b), which map a smooth curve in the QCD phase diagram — the so-called chemical freeze-out curve. BES-I filled the gaps in the energies between old RHIC and SPS. The baryon chemical potential decreases with energy increasing reflecting nuclear transparency and low-rich net baryon density QGP. The chemical freeze-out temperature increases with energy increasing till saturating at limiting temperature $T_{\lim} = (158.5 \pm 3)$ MeV. This possibly means — as the energy increases, the system produces more particles rather than increases its temperature.

The discovery of new resonances, especially with low masses, will affect the extracted freeze-out parameters. The cut in resonance masses of 2 GeV gives us the same results. For single hard-core radius of hadrons, the EVC is practically irrelevant when extracting the chemical freeze-out parameters, although it modifies the thermodynamic quantities. The feed-down from weak decay reaches asymptotic values of 15, 25 and 35% for pion, lambda and proton, respectively [4]. It is also significantly large for antiparticles at high energies. The inclusion of the feed-down contributions should be implemented [4]. The closeness between lattice QCD pseudocritical temperature [12] and its leading-order correction in μ_b/T [48] and the HRG model parameters insure that the validity of the HRG model in the hadronic phase and time chemical freeze-out occurs at phase transition.

REFERENCES

1. *Cabibbo N., Parisi G.* Exponential Hadronic Spectrum and Quark Liberation // Phys. Lett. B. 1975. V. 59. P. 67.

2. *Gyulassy M., McLerran L.* New Forms of QCD Matter Discovered at RHIC // Nucl. Phys. A. 2005. V. 750. P. 30.

3. *Tawfik A.* Equilibrium Statistical-Thermal Models in High-Energy Physics // Intern. J. Mod. Phys. A. 2014. V. 29. P. 1430021.

4. *Andronic A., Braun-Munzinger P., Stachel J.* Hadron Production in Central Nucleus–Nucleus Collisions at Chemical Freeze-Out // Nucl. Phys. A. 2006. V. 772. P. 167.

5. *Becattini F. et al.* Features of Particle Multiplicities and Strangeness Production in Central Heavy-Ion Collisions between $1.7A$ and $158A$ GeV/c // Phys. Rev. C. 2001. V. 64. P. 024901.

6. *Cleymans J., Satz H.* Thermal Hadron Production in High-Energy Heavy-Ion Collisions // Z. Phys. C. 1993. V. 57. P. 135.

7. *Tawfik A.* Particle Ratios in Heavy-Ion Collisions // Fizika B. 2009. V. 18. P. 141;
Tawfik A. Antiproton-to-Proton Ratios for ALICE Heavy-Ion Collisions // Nucl. Phys. A. 2011. V. 859. P. 63.

8. *Torrieri G. et al.* SHARE: Statistical Hadronization with Resonances // Comp. Phys. Commun. 2005. V. 167. P. 229.

9. *Tiwari S. K., Singh C. P.* Particle Production in Ultrarelativistic Heavy-Ion Collisions: A Statistical-Thermal Model Review // Adv. High Energy Phys. 2013. V. 2013. P. 805413.

10. *Yen G. D. et al.* Excluded-Volume Hadron Gas Model for Particle Number Ratios in $A + A$ Collisions // Phys. Rev. C. 1997. V. 56. P. 2210;
Begun V. V., Gazdzicki M., Gorenstein M. I. Hadron-Resonance Gas at Freeze-Out: Reminder on Importance of Repulsive Interactions // Phys. Rev. C. 2013. V. 88. P. 024902.

11. *Aggarwal M. M. et al. (STAR Collab.).* An Experimental Exploration of the QCD Phase Diagram: The Search for the Critical Point and the Onset of Deconfinement. 1007.2613 [nucl-ex].

12. *Bazavov A. et al.* Chiral and Deconfinement Aspects of the QCD Transition // Phys. Rev. D. 2012. V. 85. P. 054503.

13. *Hagedorn R.* Lectures on Thermodynamics of Strong Interactions. CERN Report 71-12. 1971.

14. *Karsch F., Redlich K., Tawfik A.* Hadron Resonance Mass Spectrum and Lattice QCD Thermodynamics // Eur. Phys. J. C. 2003. V. 29. P. 549.

15. *Karsch F., Redlich K., Tawfik A.* Thermodynamics at Nonzero Baryon Number Density: A Comparison of Lattice and Hadron Resonance Gas Model Calculations // Phys. Lett. B. 2003. V. 571. P. 67.

16. *Redlich K., Karsch F., Tawfik A.* Heavy-Ion Collisions and Lattice QCD at Finite Baryon Density // J. Phys. G. 2004. V. 30. P. S1271.

17. *Tawfik A.* QCD Phase Diagram: A Comparison of Lattice and Hadron Resonance Gas Model Calculations // Phys. Rev. D. 2005. V. 71. P. 054502.

18. *Tawfik A.* The Influence of Strange Quarks on QCD Phase Diagram and Chemical Freeze-Out: Results from the Hadron Resonance Gas Model // J. Phys. G. 2005. V. 31. P. S1105.

19. *Venugopalan R., Prakash M.* Thermal Properties of Interacting Hadrons // Nucl. Phys. A. 1992. V. 546. P. 718.

20. *Becattini F.* Universality of Thermal Hadron Production in pp, $p\bar{p}$ and e^+e^- Collisions. arXiv:hep-ph/9701275;
Becattini F. Thermal Hadron Production in High-Energy Collisions // J. Phys. G. 1997. V. 23. P. 1933.

21. *Letessier J., Rafelski J.* Hadron Production and Phase Changes in Relativistic Heavy-Ion Collisions // Eur. Phys. J. A. 2008. V. 35. P. 221.

22. *Becattini F., Heinz U. W.* Thermal Hadron Production in pp and $p\bar{p}$ Collisions // Z. Phys. C. 1997. V. 76. P. 269; Erratum // Ibid. P. 578.

23. *Kraus I. et al.* Particle Production in $p-p$ Collisions at $\sqrt{s} = 17$ GeV within the Statistical Model // Phys. Rev. C. 2010. V. 81. P. 024903.

24. *Becattini F.* A Thermodynamical Approach to Hadron Production in e^+e^- Collisions // Z. Phys. C. 1996. V. 69. P. 485.

25. *Becattini F. et al.* Hadron Formation in Relativistic Nuclear Collisions and the QCD Phase Diagram // Phys. Rev. Lett. 2013. V. 111. P. 082302;
Stock R. et al. Hadronic Freeze-Out in $A + A$ Collisions Meets the Lattice QCD Parton–Hadron Transition Line // PoS. CPOD2013. 2013. 011.

26. *Beringer J. et al. (Particle Data Group)* // Phys. Rev. D. 2012. V. 86. P. 010001.

27. *Michalec M.* Thermal Description of Particle Production in Ultrarelativistic Heavy-Ion Collisions. arXiv:nucl-th/0112044.

28. *Michalec M., Florkowski W., Broniowski W.* Scaling of Hadron Masses and Widths in Thermal Models for Ultrarelativistic Heavy-Ion Collisions // Phys. Lett. B. 2001. V. 520. P. 213.

29. *Petran M. et al.* Hadron Production and QGP Hadronization in Pb–Pb Collisions at $\sqrt{s_{NN}} = 2.76$ TeV // Phys. Rev. C. 2013. V. 88. P. 034907.

30. *Landau L. D., Lifshitz E. M.* Statistical Physics. Pergamon: Oxford, 1975.

31. *Tawfik A.* Constant-Trace Anomaly as a Universal Condition for the Chemical Freeze-Out // Phys. Rev. C. 2013. V. 88. P. 035203.

32. *Braun-Munzinger P., Heppe I., Stachel J.* Chemical Equilibration in Pb + Pb Collisions at the SPS // Phys. Lett. B. 1999. V. 465. P. 15;
Braun-Munzinger P. et al. Thermal and Hadrochemical Equilibration in Nucleus–Nucleus Collisions at the SPS // Phys. Lett. B. 1996. V. 365. P. 1.

33. *Borsnyi Sz. et al.* QCD Equation of State at Nonzero Chemical Potential: Continuum Results with Physical Quark Masses at Order μ^2 // JHEP. 2012. V. 1208. P. 053.

34. *Becattini F. et al.* Chemical Equilibrium Study in Nucleus–Nucleus Collisions at Relativistic Energies // Phys. Rev. C. 2004. V. 69. P. 024905;
Andronic A. et al. The Statistical Model in Pb–Pb Collisions at the LHC // Nucl. Phys. A. 2013. V. 904. P. 535c.

35. *Markert C. (for the STAR Collab.).* Strange Resonance Production in $p + p$ and Au + Au Collisions at RHIC Energies // J. Phys. G. 2004. V. 30. P. S1313.

36. *Ullrich T.* Experimental Summary on Global Observables, Hadron Spectra and Ratios // Nucl. Phys. A. 2003. V. 715. P. 399.

37. *Cleymans J.* Theoretical Status on Strangeness Production // The 3rd Intern. Conf. on Phys. and Astrophys. of Quark Gluon Plasma (ICPAQGP 97), Jaipur, India, 1997.

38. *Abelev B. I. et al. (STAR Collab.).* Systematic Measurements of Identified Particle Spectra in pp, $d + $Au and Au + Au Collisions from STAR // Phys. Rev. C. 2009. V. 79. P. 034909.

39. *Adams J. et al. (STAR Collab.).* Scaling Properties of Hyperon Production in Au + Au Collisions at $\sqrt{s_{NN}} = 200$ GeV // Phys. Rev. Lett. 2007. V. 98. P. 062301.

40. *Aggarwal M. M. et al. (STAR Collab.).* Strange and Multistrange Particle Production in Au + Au Collisions at $\sqrt{s_{NN}} = 62.4$ GeV // Phys. Rev. C. 2011. V. 83. P. 024901.

41. *Adler C. et al. (STAR Collab.).* Midrapidity Λ and $\bar{\Lambda}$ Production in Au + Au Collisions at $\sqrt{s_{NN}} = 130$ GeV // Phys. Rev. Lett. 2002. V. 89. P. 092301.

42. *Adams J. et al. (STAR Collab.).* Multistrange Baryon Production in Au–Au Collisions at $\sqrt{s_{NN}} =$ 130 GeV // Phys. Rev. Lett. 2004. V. 92. P. 182301.

43. *Kumar L. (for the STAR Collab.).* Identified Hadron Production from the RHIC Beam Energy Scan // J. Phys. G: Nucl. Part. Phys. 2011. V. 38. P. 124145.

44. *Das S. (for the STAR Collab.).* Centrality Dependence of Freeze-Out Parameters from the Beam Energy Scan at STAR // Nucl. Phys. A. 2013. V. 904–905. P. 891c.

45. *Zhu X. (for the STAR Collab.).* Measurements of K_s^0 Λ and Ξ from Au + Au Collisions at $\sqrt{s_{NN}} =$ 7.7, 11.5 and 39 GeV in STAR // Acta Phys. Polon. B. Proc. Suppl. 2012. V. 5. P. 213.

46. *Zhao F., Xu N.* Private Communication.

47. *Andronic A., Braun-Munzinger P., Stachel J.* Thermal Hadron Production in Relativistic Nuclear Collisions: The Hadron Mass Spectrum, the Horn, and the QCD Phase Transition // Phys. Lett. B. 2009. V. 673. P. 142; Erratum // Ibid. V. 678. P. 516.

48. *Kaczmarek O. et al.* Phase Boundary for the Chiral Transition in $(2 + 1)$-Flavor QCD at Small Values of the Chemical Potential // Phys. Rev. D. 2011. V. 83. P. 014504.